Atmos. Chem. Phys., 13, 6049–6064, 2013
www.atmos-chem-phys.net/13/6049/2013/
doi:10.5194/acp-13-6049-2013

Atmospheric Chemistry and Physics Open Access

Observation of horizontal winds in the middle-atmosphere between 30° S and 55° N during the northern winter 2009–2010

P. Baron[1], D. P. Murtagh[2], J. Urban[2], H. Sagawa[1], S. Ochiai[1], Y. Kasai[1,6], K. Kikuchi[1], F. Khosrawi[3], H. Körnich[4], S. Mizobuchi[5], K. Sagi[2], and M. Yasui[1]

[1]National Institute of Information and Communications Technology, 4-2-1 Nukui-kitamachi, Koganei, Tokyo 184-8795, Japan
[2]Department of Earth and Space Science, Chalmers University of Technology, 41296 Göteborg, Sweden
[3]Department of Meteorology Stockholm University, 10691 Stockholm, Sweden
[4]SMHI, Folkborgsvägen 17, 60176 Norrköping, Sweden
[5]Japan Aerospace Exploration Agency, Tsukuba, 305-8505 Japan
[6]Tokyo Institute of Technology, 4259 Nagatsuta-cho, Midori-ku, Yokohama, Kanagawa 226-8503, Japan

Correspondence to: P. Baron (baron@nict.go.jp)

Received: 17 October 2012 – Published in Atmos. Chem. Phys. Discuss.: 17 December 2012
Revised: 17 May 2013 – Accepted: 17 May 2013 – Published: 25 June 2013

Abstract. Although the links between stratospheric dynamics, climate and weather have been demonstrated, direct observations of stratospheric winds are lacking, in particular at altitudes above 30 km. We report observations of winds between 8 and 0.01 hPa (∼ 35–80 km) from October 2009 to April 2010 by the Superconducting Submillimeter-Wave Limb-Emission Sounder (SMILES) on the International Space Station. The altitude range covers the region between 35–60 km where previous space-borne wind instruments show a lack of sensitivity. Both zonal and meridional wind components were obtained, though not simultaneously, in the latitude range from 30° S to 55° N and with a single profile precision of 7–9 $m\,s^{-1}$ between 8 and 0.6 hPa and better than 20 $m\,s^{-1}$ at altitudes above. The vertical resolution is 5–7 km except in the upper part of the retrieval range (10 km at 0.01 hPa). In the region between 1–0.05 hPa, an absolute value of the mean difference $< 2\,m\,s^{-1}$ is found between SMILES profiles retrieved from different spectroscopic lines and instrumental settings. Good agreement (absolute value of the mean difference of $\sim 2\,m\,s^{-1}$) is also found with the European Centre for Medium-Range Weather Forecasts (ECMWF) analysis in most of the stratosphere except for the zonal winds over the equator (difference $> 5\,m\,s^{-1}$). In the mesosphere, SMILES and ECMWF zonal winds exhibit large differences ($> 20\,m\,s^{-1}$), especially in the tropics. We illustrate our results by showing daily and monthly zonal wind variations, namely the semi-annual oscillation in the tropics and reversals of the flow direction between 50–55° N during sudden stratospheric warmings. The daily comparison with ECMWF winds reveals that in the beginning of February, a significantly stronger zonal westward flow is measured in the tropics at 2 hPa compared to the flow computed in the analysis (difference of $\sim 20\,m\,s^{-1}$). The results show that the comparison between SMILES and ECMWF winds is not only relevant for the quality assessment of the new SMILES winds, but it also provides insights on the quality of the ECMWF winds themselves. Although the instrument was not specifically designed for measuring winds, the results demonstrate that space-borne sub-mm wave radiometers have the potential to provide good quality data for improving the stratospheric winds in atmospheric models.

1 Introduction

Stratospheric winds play an important role in stratospheric chemistry by transporting long-lived species, or by creating transport barriers that, for example, isolate the polar vortex in winter (Shepherd, 2007, 2008). The stratospheric Quasi-biennial Oscillation (QBO) and downward feedback from the stratospheric vortex to tropospheric weather systems have also been reported to be relevant both in the context of weather prediction and climate (Baldwin and Dunkerton, 1999; Baldwin et al., 2003;

Sigmond et al., 2008; Marshall and Scaife, 2009; Wang and Chen, 2010). In addition, stratospheric winds describe and affect vertically propagating atmospheric waves that control the transport circulation in the stratosphere and mesosphere (Holton and Alexander, 2000).

In meteorological analyses and reanalyses, unobserved variables are constrained by observed ones through the use of balance relationships. The application of a mass-wind balance (Derber and Bouttier, 1999) leads to a state where the large number of temperature soundings provide a strong constraint on the balanced wind component, i.e. approximately the geostrophic wind. However, it is difficult to derive the larger scale wind fields using the geostrophic assumption in the tropics because the Coriolis parameter vanishes at the equator and the solutions become numerically unstable (Hamilton, 1998; Žagar et al., 2004; Polavarapu et al., 2005). For instance, significant differences are seen between wind climatologies derived from mass balance (Fleming et al., 1990; Randel et al., 2004). A further complication in the middle atmosphere is that the small errors from the lower atmosphere propagate vertically and amplify strongly in the upper stratosphere and mesosphere (Nezlin et al., 2009; Alexander et al., 2010). Thus, in order to constrain middle atmospheric winds in meteorological analyses, global wind observations in the middle atmosphere are essential. Lahoz et al. (2005) have shown that wind observations on a global scale with a precision of $5\,\mathrm{m\,s^{-1}}$ between 25 and 40 km would provide significant improvements of zonal-wind analyses especially in the tropical middle and upper stratosphere (50–1 hPa).

In spite of the importance of middle atmospheric observations, wind measurements assimilated in the models are mostly limited to the troposphere. In the mesosphere, winds are measured using optical techniques from satellites (Shepherd et al., 1993; Hays et al., 1993; Killeen et al., 1999; Swinbank and Ortland, 2003; Niciejewski et al., 2006) and by ground-based radar systems such as European Incoherent SCATter (EISCAT) (Alcaydé and Fontanari, 1986) and various meteor radars (Maekawa et al., 1993; Jacobi et al., 2009). Wu et al. (2008) have used the microwave oxygen line at 118 GHz measured by the Microwave Limb Sounder (MLS) to derive line-of-sight winds in the mesosphere (70–92 km). The authors suggested that winds can be derived down to 40 km by using emission lines from other molecules, but no results have been shown yet. Stratospheric winds have been measured from the ground using active and passive techniques (Hildebrand et al., 2012; Rüfenacht et al., 2012) and from space by the High Resolution Doppler Imager (HRDI) on UARS covering 10–35 km and 60° S–60° N, using the molecular oxygen A- and B-bands (Ortland et al., 1996).

Figure 1 summarises previous and planned wind measuring instruments from spaceborne platforms. A gap in the coverage of high quality winds ($< 5\,\mathrm{m\,s^{-1}}$ error) between 30 and 60 km clearly exists. The ESA Atmospheric Dynamics Mission on the Aeolus satellite is planned for 2013–2014 (Stoffelen et al., 2005) for measuring winds in the troposphere and lower stratosphere using a UV lidar. For middle-stratospheric winds, the Stratospheric Wind Interferometer For Transport studies (SWIFT) instrument was planned by the Space Canadian Agency for 2010 (McDade et al., 2001), but has an unclear future at the time of writing. The target of SWIFT is to measure the thermal emission from O_3 lines at 8 µm in order to provide winds on a near global scale between 15–50 km with the best accuracy of $3–5\,\mathrm{m\,s^{-1}}$ between 20–40 km and a vertical resolution of 2 km.

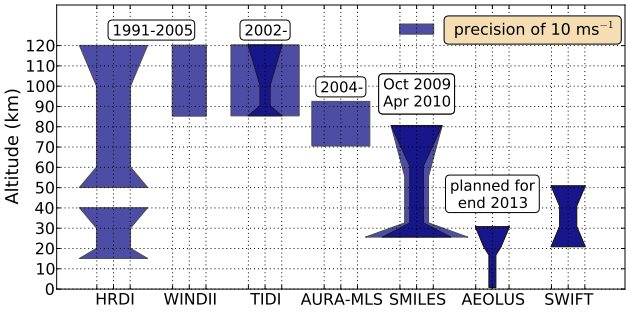

Fig. 1. The height coverage and estimated precision of past, current and future wind measuring instruments: reported validated precisions are in blue and theoretical values are in darker blue. HRDI (Ortland et al., 1996) and WINDII (Shepherd et al., 1993) were on the UARS satellite and operated from September 1991–June 2005, TIDI (Niciejewski et al., 2006) operates on the TIMED satellite from 2002-present, AURA-MLS (Wu et al., 2008) operates on the AURA satellite from July 2004–present (note that wind is not a standard product), SMILES operated on the ISS from September 2009–April 2010, Aeolus is ESA mission (Stoffelen et al., 2005) planned for 2013 and SWIFT (McDade et al., 2001) is under study in Canada.

Here we report the first spaceborne observations of winds in the altitude gap 30–60 km using the Superconducting Submillimeter-Wave Limb-Emission Sounder (SMILES) onboard the Japanese Experiment Module (JEM) of the International Space Station (ISS) (Kikuchi et al., 2010; Ochiai et al., 2012b). The instrument has been conceived for measuring trace gas profiles and was launched in September 2009. Although SMILES was not designed for this purpose, we have exploited its high frequency resolution and high signal-to-noise ratio to derive the small Doppler shifts in the atmospheric spectra and thereby line-of-sight wind velocities. Because of the ISS rotation during an orbit, components near the meridional and the zonal directions are retrieved between 30° S–55° N. As shown in this analysis, the wind information is derived from 8–0.01 hPa (∼ 35–80 km) with a precision better than $10\,\mathrm{m\,s^{-1}}$ at altitudes between 6 and 0.5 hPa and better than $20\,\mathrm{m\,s^{-1}}$ at altitudes above.

The main purpose of this paper is to present the wind data that have been derived from the six months of SMILES observations (October 2009 to April 2010) as well as assessing their quality. A further purpose is to compare the

SMILES measurements with the operational wind analysis by the European Centre for Medium-Range Weather Forecasts (ECMWF). At mid-latitudes in the middle-stratosphere, ECMWF winds are expected to provide a wind representation with an error smaller than that of a SMILES single retrieval and, thus, to provide a good dataset to check the SMILES wind quality. On the other hand, ECMWF results are uncertain in the middle and upper stratosphere of the tropical regions (Baldwin and Gray, 2005). The spread of a perturbed Ensemble of Data Assimilations (EDA) at ECMWF indicates a precision of about $3\,\mathrm{m\,s^{-1}}$ for the tropical middle-stratospheric zonal winds (Isaksen et al., 2010). The EDA method does not give information about the accuracy, and because of the lack of other stratospheric wind measurements, SMILES data offer a unique opportunity to estimate it.

In Sect. 2, we briefly describe the measurement method. The theoretical precision (random errors) and accuracy (systematic errors) are estimated from a sensitivity study. Section 3 assesses the quality of the SMILES data by checking the internal consistency of the different SMILES products and their mean differences with the ECMWF winds. In Sect. 4, the results are illustrated with monthly global maps and the daily variation of the zonal-winds. Both the measured Semi-Annual Oscillations (SAO) of the zonal-wind above the Equator, and the zonal-wind reversals between 50–55° N during Arctic Sudden Stratospheric Warming (SSW) events are discussed and are compared with the ECMWF analysis. Finally, we summarise our results and give conclusions as well as discuss ongoing work for improving the SMILES winds.

2 SMILES observations

2.1 Measurement method

SMILES was attached to the ISS in Sept 2009 and functioned for 7 months until April 2010. It observed the Earth's limb, scanning from −7 to 100 km in 53 s, providing 1600 spectral radiance profiles per day. Using Superconductor-Insulator-Superconductor (SIS) detectors cooled at 4 K, it provided high quality spectra allowing constituent profiles of many species such as ozone (O_3) and hydrogen chloride (HCl) to be derived (Kasai et al., 2006; Takahashi et al., 2010; Khosravi et al., 2012; Kasai et al., 2013). SMILES observed spectral lines from the atmospheric limb in three frequency bands, named A (624.3–625.5 GHz), B (625.1–626.3 GHz) and C (649.1–650.3 GHz) but only two are measured simultaneously. Two acousto-optical spectrometers (AOS-1 and AOS-2) with similar specifications are used. Frequency calibration and stability are ensured using an ultra-stable oscillator and frequent comb calibration of the AOS (Mizobuchi et al., 2012b). Inherent in the spectra is information on the Doppler shift caused by the ISS ($\sim 4\,\mathrm{km\,s^{-1}}$ along the line of sight) as well as atmospheric motion. The broadening of the spectral lines into several spectral channels provides enough sensitivity to detect the small frequency shift induced by the winds (e.g. a $50\,\mathrm{m\,s^{-1}}$ line-of-sight wind induces a shift of 100 kHz which has to be compared to the spectrometer spectral resolution of 1.2 MHz and to the full-width-half-maximum of the spectral line that decreases from ∼ 50 MHz at 10 hPa to ∼ 1 MHz at 0.2 hPa). For deriving wind, the two strongest spectral lines have been used separately. One is an emission line of O_3 at 625.371 GHz common to bands A and B, and the second one is a $H^{35}Cl$ triplet at 625.92 GHz (band B). Hence, three wind profiles are independently retrieved, two from the O_3 line in bands A and B, and one from the HCl triplet in band B. The wind retrieval algorithm is similar to the one presented in Baron et al. (2011) for the temperature and trace gas profiles retrieval (see Appendix for more details). Profiles of geophysical parameters are retrieved from the inversion of the set of spectra that are measured during a single vertical scan of the atmospheric limb. To simplify and speed-up the retrieval calculations, the same line-of-sight velocity is removed from all spectra composing a vertical scan. The velocity which changes from one scan to another, is chosen at the middle of the scan. After the retrieval calculation, the derived wind profile is corrected from the altitude variation of the line-of-sight velocity ($\sim 0.8\,\mathrm{m\,s^{-1}\,km^{-1}}$).

As seen in Fig. 2, because of the geometry of the instrument field-of-view in relation to the ISS orbit, the line-of-sight winds during the ascending (descending) portion of an orbit are almost in meridional (zonal) direction. Figure 3 shows single line-of-sight wind retrievals at 36 km on 2 and 26 January for both ascending and descending portions of the orbits. Between ∼ 30° S to ∼ 55° N, the line-of-sight direction do not deviate by more than 10° from the exact zonal or meridional directions. The full latitude range of observations is between 38° S and 65° N but on the borders, the line-of-sight rotates quickly and deviates from the meridional or zonal direction. Another characteristic of the observations is, as the result of the 2 months periodic local-time precession of the ISS, semidiurnal and diurnal variations of mesospheric winds such as those induced by tides are captured in the observations.

2.2 Theoretical estimation of the retrieval errors

Figure 4 (left panel) shows the vertical resolution of the retrieved wind profiles and the measurement responses, i.e., the sum of the averaging kernel rows (Merino et al., 2002) that indicate the altitudes of good measurement sensitivity. Good sensitivity (defined as where the measurement response ranges from 0.9 to 1.1) is found from 25 to 70 km (20–0.05 hPa) and from 25 to 80 km (20–0.01 hPa) for the O_3 and HCl line retrievals, respectively. In the mesosphere, the steep decrease of the O_3 concentration is responsible of the loss of the retrieval sensitivity from the O_3 line and the HCl lines, though weaker in the stratosphere, become more suitable because the HCl VMR profile has its maximum in

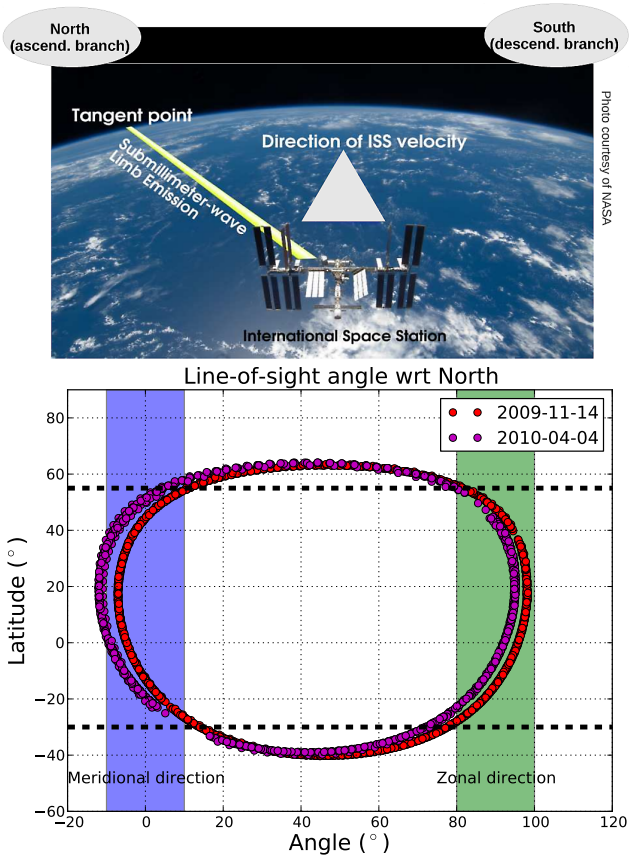

Fig. 2. Upper panel: Representation of the limb observation geometry (adapted from http://smiles.nict.go.jp/pub/about/principles.html). The ISS orbit inclination is 51.6° with respect to the equator and the SMILES line-of-sight is tilted by 45° on the left side of the forward direction. The tangent point is at a distance of ∼2000 km from the ISS. North (South) direction is indicated for the ascending (descending) orbit branch. Lower panel: latitudinal variation of the line-of-sight angle with respect to the North direction on 14 November 2009 (red circles) and on 4 April 2010 (magenta circles). The blue (green) region indicates the region where the line-of-sight is between ±10° about the meridional (zonal) direction. The thick dashed horizontal lines indicate the latitude range between 30° S and 55° N.

the upper-stratosphere and lower-mesosphere, and the HCl spectrum is composed of three relatively strong spectral lines within a narrow range of 30 MHz. According to the vertical resolution of the retrieved profiles, the best information is obtained from the O_3 line below 60 km (0.2 hPa), and from the HCl lines at altitudes above. The vertical resolution of the composite retrieved profile is 5–7 km up to 70 km and increases to 10 km at 80 km. Since the wind information comes from a layer of 5 to 10 km thickness around the line-of-sight tangent point, the horizontal resolution along the line-of-sight is between 500 and 700 km.

The theoretical precision and accuracy for a single profile retrieval are shown in the central and right panels of Fig. 4, respectively. The methodology and the assumptions of the error analysis are given in Baron et al. (2011), except for the errors on the calibration parameters which include a correction for a nonlinearity in the receiver which was not applied in the previous analysis (Ochiai et al., 2012a). An error of 20 % is assumed on the nonlinear parameters. The retrieval precision is limited by the measurement noise and to a lesser extent by the uncertainties in the O_3 and HCl abundances. The theoretical precision is 4–10 $\mathrm{m\,s^{-1}}$ between 35 and 60 km (O_3 line retrieval) and $< 20\,\mathrm{m\,s^{-1}}$ between 60 and 80 km (HCl line retrieval). The accuracy of the retrieval at lower altitudes is set by systematic effects on the ozone line retrieval (dashed black line), in particular errors on the intensity calibration of the spectra.

In summary, although the retrieval sensitivity reaches down to 25 km, good quality wind profiles (accuracy $< 5\,\mathrm{m\,s^{-1}}$) are actually retrieved above 35 km (8 hPa). The upper limit of the retrieval is 80 km using the band-B HCl lines.

2.3 Data selection and ECMWF wind pairing

In this analysis, retrieved winds with a measurement response smaller than 0.9 are rejected. The retrieval quality is estimated from a χ^2 defined as the sum of the squares of the spectral fit residual weighted by the corresponding measurement errors and divided by the total number of measurements (Eq. 2 in Baron et al. (2011)). For regularising the inversion, an a priori knowledge of the winds is used in the χ^2 which can be considered as additional virtual measurements (see Appendix A). Abnormally high values of the χ^2 before the retrieval indicate scans possibly affected by errors such as obstructions in the field-of-view or inaccurate instrument pointing information. High values of the χ^2 after the retrieval indicate bad measurement fit. The values of the χ^2 before and after the retrieval are both checked since the scans with errors can be fitted effectively but with incorrect wind values. For the O_3 line in band-A (band-B), retrievals with a normalized χ^2 larger than 40 (30) before the inversion or larger than 2 (1.5) after the inversion are rejected. For the HCl line in band-B, the χ^2 thresholds for rejection are 50 before inversion and 2.5 after inversion.

ECMWF operational analysis data were used starting with Integrated Forecasting system (IFS) cycle 35 release 3 in September 2009. In this version, the mesospheric winds were significantly improved by using a nonorographic gravity wave scheme (Orr et al., 2010). A major operational upgrade occurred in the middle of the mission on 26 January 2010, when cycle 36 release 1 was introduced with an increase of the model resolution from T799 to T1279 from 25 km to 16 km. To compare the measurements with the ECMWF analysis, the SMILES profiles are paired with the closest ECMWF profile in space and time. ECMWF analyses were extracted on a latitude-longitude grid of $0.5 \times 0.5°$

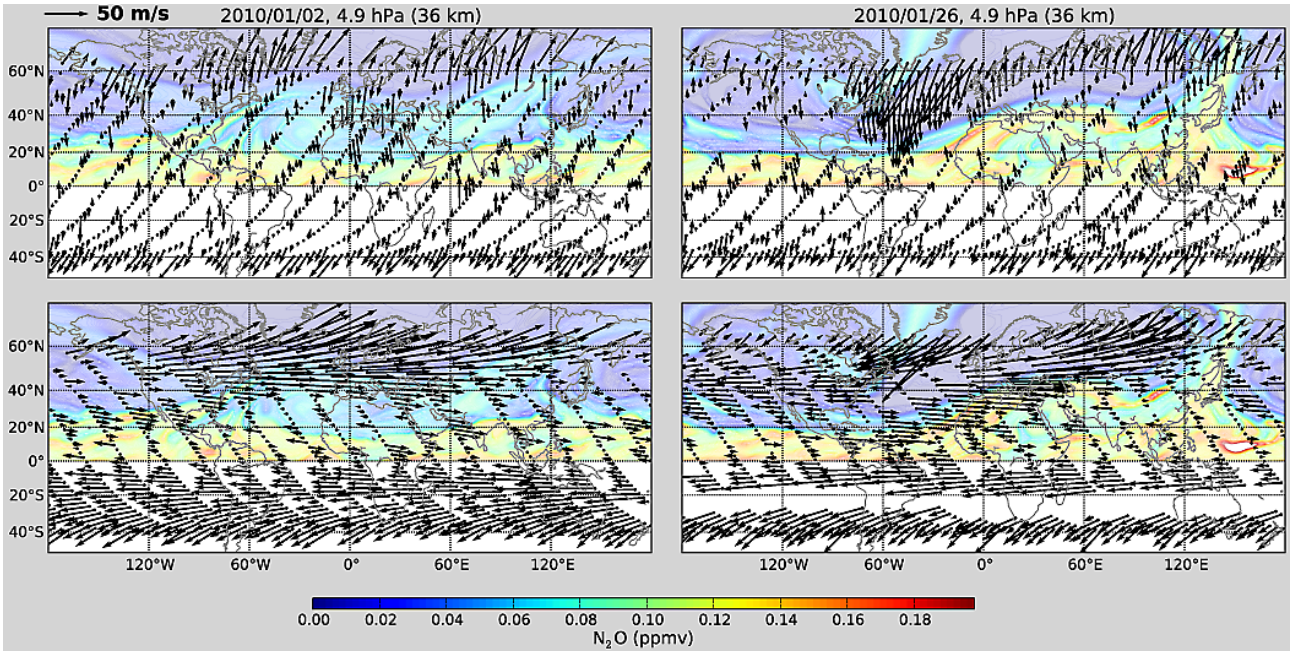

Fig. 3. Typical line-of-sight wind vectors retrieved at 5 hPa (∼ 36 km) on 2 January 2010 (left column) and on 26 January 2010 (right column). The orientation of the arrows is that of the wind component along the line-of-sight. The length of the arrows is proportional to the amplitude of the corresponding line-of-sight wind (the same proportional factor is applied at all latitudes). The upper (lower) panels correspond to the ascending (descending) branch of the orbit where the line-of-sight is near the meridional (zonal) direction between ∼ 35° S to ∼ 55° N. The background colour shows the northern N_2O distribution from the assimilated Odin/SMR measurements in a model driven by ECMWF winds at the isentropic surface of 850 K.

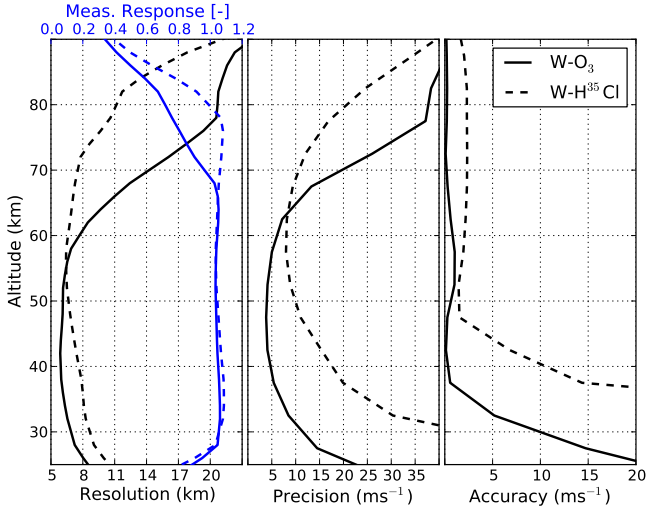

Fig. 4. Left panel: vertical resolution (dark line) and measurement response (blue line) for line-of-sight wind profiles retrieved from the O_3 spectral line (full lines) and from the $H^{35}Cl$ triplets in band B (dashed lines). Central panel: estimates of line-of-sight wind single retrieval precision derived from the O_3 spectral line (full line) and the $H^{35}Cl$ triplets (dashed line). Right panel: same as central panel but for the accuracy.

and 4 times per day, which corresponds to coincidence criteria of 3 h and 0.25°. The profiles extend up to 0.01 hPa (∼ 80 km) with a vertical resolution of about 1.5 km in the middle stratosphere. The component of the ECMWF winds parallel to the SMILES line-of-sight is computed with the vertical resolution degraded to that of the retrieved profiles based on the shape of the retrieval averaging kernels.

2.4 Zero-wind correction

Errors which are not significant for trace gas retrieval have not been fully characterised properly and were not included in the error analysis described in Sect. 2.2. However, wind retrievals are sensitive to some of these errors such as the spectrometer frequency calibration, the main local-oscillator frequency, the line-of-sight velocity correction and knowledge of the spectroscopic line frequency. The systematic component of these errors is mitigated by subtracting a daily "zero-wind" profile consisting of the average of observations near the meridional direction (±10°) and located in the tropics (±20° from the equator) where the actual flow is predominantly zonal. Since the meridional wind is not truly zero, a similar zero-wind computed with the paired ECMWF data is removed from the observed zero-wind. Note that the latitude range of ±20° has been defined to minimise the atmospheric contribution in the zero-wind based on estimations using the

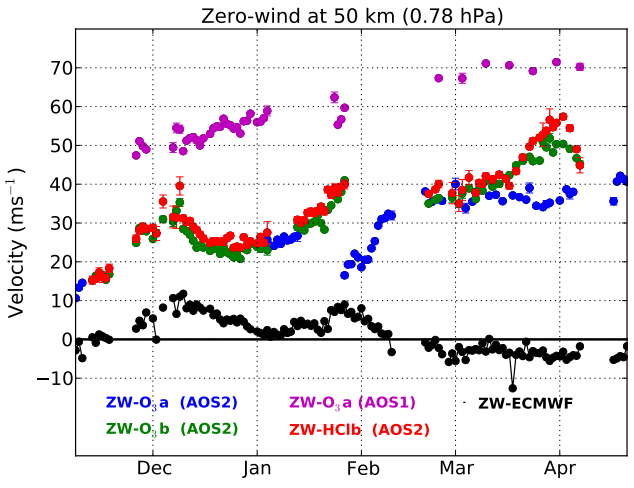

Fig. 5. Zero-wind for bias correction derived at 50 km from the O_3 line in band-A using spectrometer 1 (magenta dots) and spectrometer 2 (blue dots), the O_3 line in band-B and spectrometer 2 (green dots) and HCl line in band-B (red dots) along with the zero-wind computed with the paired ECMWF winds. The error bar corresponds to the retrieval errors of the averaged profiles (1-σ). The zero-wind includes the subtraction of the ECMWF zero-winds.

ECMWF winds. Figure 5 shows the zero-winds at 50 km derived from the three SMILES products. At this altitude, the three products are retrieved with a good sensitivity and the spectrometer frequency error is expected to be the main measurement bias. For lines in band-B, which is always measured with the second spectrometer unit (AOS-2), the zero-wind corrections vary between 20–50 m s^{-1} and the day-to-day changes do not exceed 5 m s^{-1}. The zero-wind correction retrieved from the O_3 line in band-A shows two regimes depending which spectrometer is used. When the first spectrometer unit (AOS-1) is used for the measurements (configuration for measuring band-B simultaneously), the zero-wind correction values are between 50–70 m s^{-1}. When band-A is measured with AOS-2, the zero-wind values are similar to those obtained for band-B. After removing the atmospheric wind variability estimated using ECMWF winds (ECMWF zero-wind in Fig. 5), a linear trend of ~ 20 m s^{-1}/6-months is seen on the 4 observational configurations (not shown). This trend is compatible with the main local-oscillator stability expected to be $\frac{\delta_\nu}{\nu} = 6.8 \times 10^{-8}$/6-months where ν is the local oscillator frequency. Zero-wind corrections relevant to band B oscillate with a period of 2 months and an amplitude of 10–20 m s^{-1}. Although the period is compatible with that of the instrument thermal variation, the origin of the oscillation on the band-B zero-wind is not yet fully understood.

Such frequency offsets (< 0.1 MHz) are acceptable for trace gas retrievals which are the first objective of the mission. However, it is clearly not good enough for wind retrieval which requires the "zero-wind" correction. However, as seen by the ECMWF zero-wind, during some periods between December and February the atmospheric contribution in the zero-wind correction can reach ~ 10 m s^{-1} which would introduce a bias in the wind profile if solely corrected with the retrieved zero-wind value. Above 0.01 hPa, ECMWF winds are not available and are linearly extrapolated.

3 Data quality assessment and comparison with ECMWF analysis

The data quality assessment consists, first, of checking the internal consistency of the SMILES winds derived from different spectroscopic lines and spectrometers. For further verification, retrieved winds need to be compared with independent wind information. Lacking other measurements in the middle and upper stratosphere, such information is taken from the operational ECMWF analyses. It is known that, at high altitudes, tropical ECMWF winds are poorly constrained. Baldwin and Gray (2005) have compared ECMWF ERA-40 reanalysis zonal-winds with observations from two tropical stations. They found good agreement below 2–3 hPa but, at higher altitudes, their conclusion was that the reanalysis winds should be used with caution (correlation of 0.3 at 0.1 hPa with observations). Although this analysis is based on an outdated version of the ECMWF (version cy23r4), these results may still be valid and highlight the difficulties for reproducing winds in the tropics. Hence, the comparison of SMILES with ECMWF winds is not only relevant for the SMILES wind quality assessment but it also provides insights on the quality of the ECMWF winds themselves. For full verification of the SMILES winds, the mesospheric measurements should also be validated with ground-based radar observations. However, such analysis is beyond the scope of this paper.

3.1 Internal consistency check

The upper panels of Fig. 6 show the mean meridional wind profiles in 20° latitude bins between 20° S and 60° N that have been retrieved from the O_3 lines in bands A and B (blue and green lines, respectively) and from the HCl line in band B (red line). Only measurements when bands A and B were measured simultaneously are used. This corresponds to one third of the full dataset. The retrieved winds have been corrected with the zero-wind profile.

Between 4 and 0.1 hPa, good agreement is found for winds retrieved from the O_3 lines in all latitude bands. The standard deviation of the retrieved winds (Fig. 6, lower panels) also confirms the good agreement between the O_3 retrievals in this altitude range. At lower (8–4 hPa) and upper (< 0.1 hPa) altitudes, O_3 line derived winds exhibit differences that reach ~ 10 m s^{-1} at higher latitudes.

As indicated in Sect. 2.2, in the upper retrieval range (0.1–0.01 hPa), winds retrieved from the HCl line should be

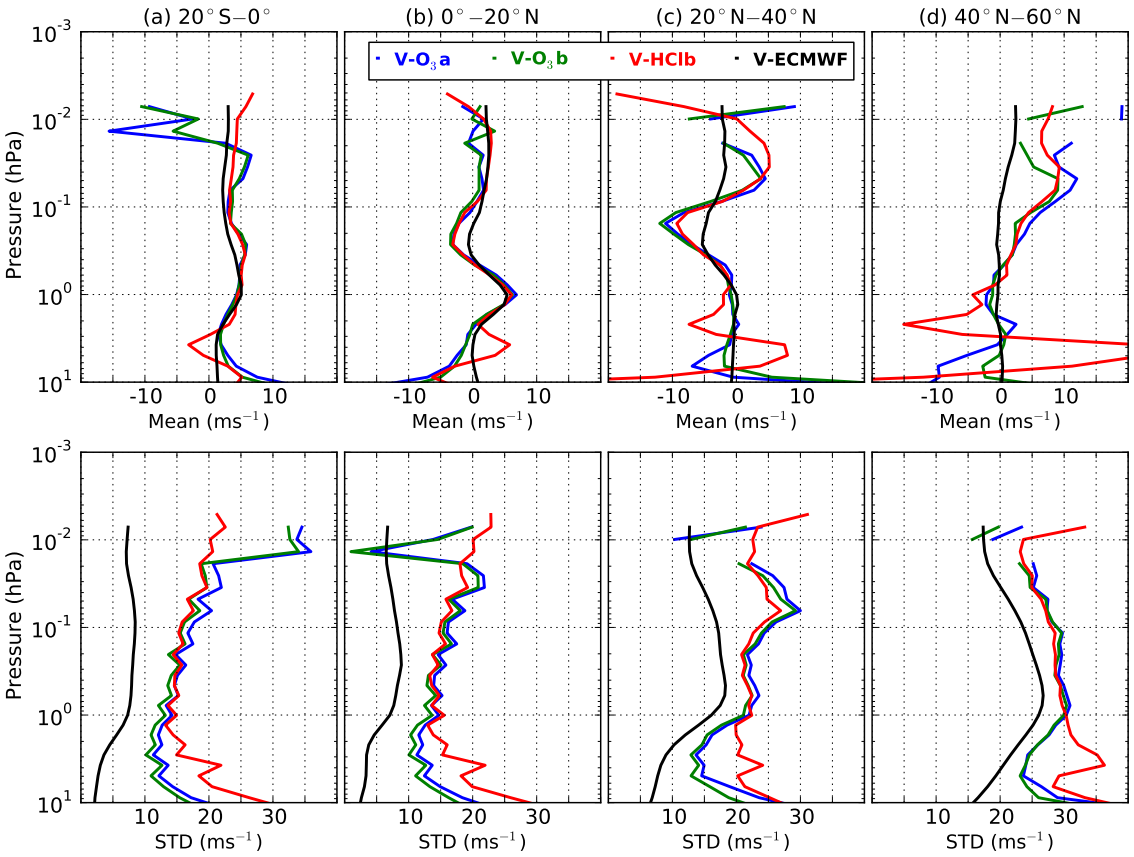

Fig. 6. Upper panels: zonally averaged near meridional wind profiles retrieved from simultaneous measurements of the spectral lines: O_3-band A (blue line), O_3-band B (red line) and HCl-band B (green line). Lower panels: same as the upper panels but showing the standard deviation of the retrieved profiles. The results for the paired ECMWF winds component along the line-of-sights are also shown (black line). Data with a line-of-sight orientation between $\pm 10°$ from the meridional direction are used.

preferred. Between 1 and 0.1 hPa, the mean and the standard deviation of the profiles retrieved from the HCl line (dashed-red line) match those from the O_3 retrievals. At higher altitudes, the mean and standard deviation of the HCl wind profiles smoothly expands up to 0.005 hPa. In the lower part of the retrieval range (> 1 hPa), large differences with O_3 retrievals can be seen as expected from the degradation of the accuracy and the precision of the HCl line retrieval.

The upper panel of Fig. 7 shows the differences between profiles retrieved from the O_3 and the HCl lines in band-B between 40 and 70 km. At 50 and 60 km, the standard deviation and the mean of the differences are 12 m s^{-1} and < 1.2 m s^{-1}, respectively. Since both profiles are derived from simultaneous measurements with the same spectrometer, the standard deviation is representative of the errors due to the measurement thermal noise. The value is consistent with the theoretical estimate: 5–8 m s^{-1} and 10 m s^{-1} for O_3 and HCl retrievals, respectively. At 70 km, the standard deviation increases to 16 m s^{-1} which is also consistent with the loss of precision for both O_3 and HCl retrievals (20 m s^{-1} and 13 m s^{-1}, respectively). The value of 16 m s^{-1} is smaller than the standard-deviation expected from the theoretical errors (root-sum-square of the errors is 24 m s^{-1}) indicating a pessimistic estimate of the theoretical error from the O_3 line. The actual mean precision of the winds derived from O_3 is likely between 12–15 m s^{-1}. Above 70 km (0.05 hPa), ozone has strong diurnal and latitudinal variations (Kasai et al., 2013) which induce large variations of the O_3 line intensity of more than an order of magnitude, and therefore, of the wind retrieval precision.

The comparison of the winds derived from the ozone line simultaneously measured in bands A and B (different spectrometers) and corrected with the zero-wind technique is shown in Fig. 7 (lower panel). The mean difference at altitudes between 40–60 km is less than 3 m s^{-1} and the standard deviation of the differences is 7 m s^{-1}. At 30 km, the mean difference and the standard deviation increase to 6 m s^{-1} and 13 m s^{-1}, respectively. Since the profiles are retrieved from the same spectral line, the measurement thermal noise is correlated at more than 90 % and the differences between the retrievals arise from errors on the spectrometer channels frequency. We checked that the difference is random from one

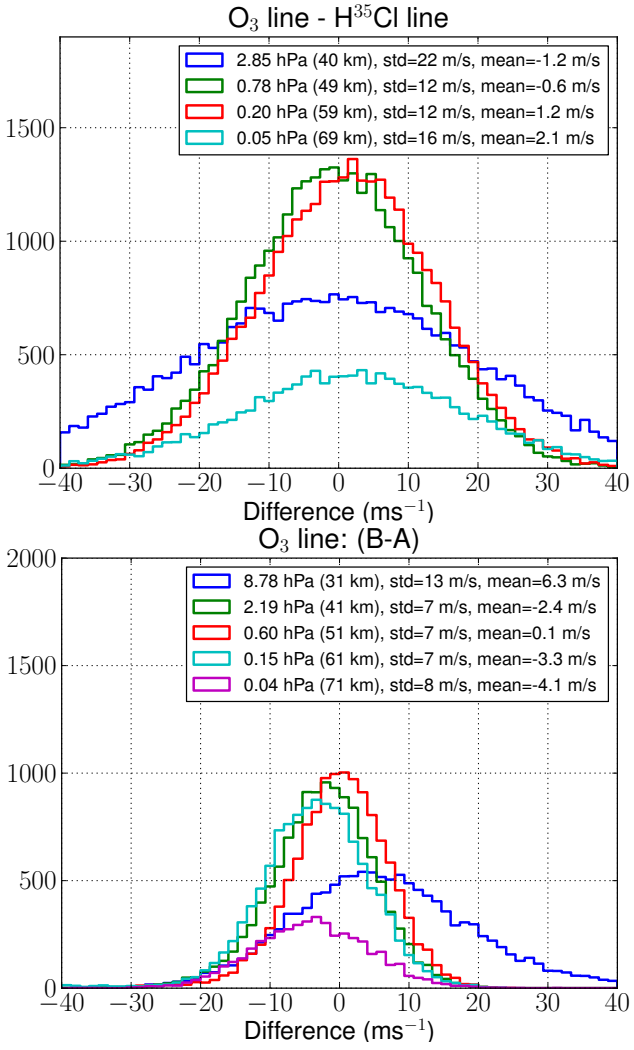

Fig. 7. Upper panel: histogram of differences of the velocity retrieved from the O_3 and the HCl lines in band B. Lower panel: same as for the left panel but for line-of-sight winds retrieved from the O_3 lines in bands A and B measured simultaneously. Data for latitudes between 20° N and 60° N have been used.

retrieval to another. Hence, the residual errors from the spectrometer channels frequency after the zero wind correction can be assumed as a random retrieval error of $\sim$5–7 m s^{-1}.

In conclusion, the different SMILES products agree with each other in the mid- and upper stratosphere where the retrieval performances are similar for each product. Our results also confirm that winds retrieved from the O_3 line should be used between 8–0.1 hPa while those obtained from the HCl line retrievals should be used between 0.1–0.01 hPa. The actual precision is significantly worse than the theoretical computation because of a residual error after the zero-wind correction. An additional noise of 5 m s^{-1} likely arises from the fluctuation in the spectrometer frequency errors. Taking into account this additional noise, the total precision of the wind retrieval becomes 7–9 m s^{-1} in the middle and upper stratosphere.

3.2 Comparison with the ECMWF meridional component

The internal checks presented in the previous section do not allow us to estimate the errors due to the platform velocity, and to the local-oscillator frequency, which affect the three wind products in the same way. However, in the tropics and extra-tropical stratosphere where meridional velocities are weak (Fig. 6), the differences between ECMWF and SMILES single profiles are caused by the retrieval errors, and, to a lesser extent, by non-coincident and non-simultaneous profile pairing and by uncertainties of ECMWF analysis. Hence the analysis of the differences between SMILES and ECMWF meridional winds in the stratosphere allows us to verify the wind retrieval error estimations. Note that large oscillations are seen on the SMILES wind profiles at low and mid-latitudes of the Northern Hemisphere which are likely due to atmospheric tides. In the mesosphere, the oscillations are significantly smaller in the ECMWF wind profiles and, consequently, the ECMWF standard deviations underestimate the actual winds variability in the mesosphere.

The mean and the standard deviation of the differences (SMILES-ECMWF) have been calculated in latitude bins of 5° for data between November 2009 and April 2010, and with a line-of-sight within ±10° around the meridional direction. We rejected the days when fewer than 10 profiles were used to construct the zero-wind profile. Figure 8 (lower panels) shows the results for the data retrieved from the O_3 line in band B. Over most of the region between 5–0.5 hPa, the bias between the model and the measurement (left panel) is less than 2 m s^{-1} and the standard deviation (right panel) is less than 10 m s^{-1}. However, the bias in the tropics should be taken with caution since the mean ECMWF tropical meridional wind is included in the zero-wind. According to these results, the precision (standard deviation) and the accuracy (bias) for a single retrieved profile cannot exceed 10 m s^{-1} and 2 m s^{-1}, respectively, which is consistent with the error estimation.

At high latitudes (40–60° N), a mean difference of 2–5 m s^{-1} is found at 4–3 hPa which may arise from the increase of the measurement bias and also from the larger variability of the meridional winds (Fig. 6). At lower altitudes (> 8 hPa) and outside the tropics, the large mean differences are due to measurement calibration errors. The calibration errors are found to be larger for the O_3 line band-A retrieval (not shown). In the mesosphere, above 0.3 hPa, results from the O_3 and the HCl lines (lower and upper panels, respectively) look very similar and the standard deviations of the differences are consistent with the increase of the measurement noise (between 13 and 20 m s^{-1}). The mean differences in the mesosphere vary between ±10 m s^{-1}. Mesospheric tides and waves may contribute to such differences.

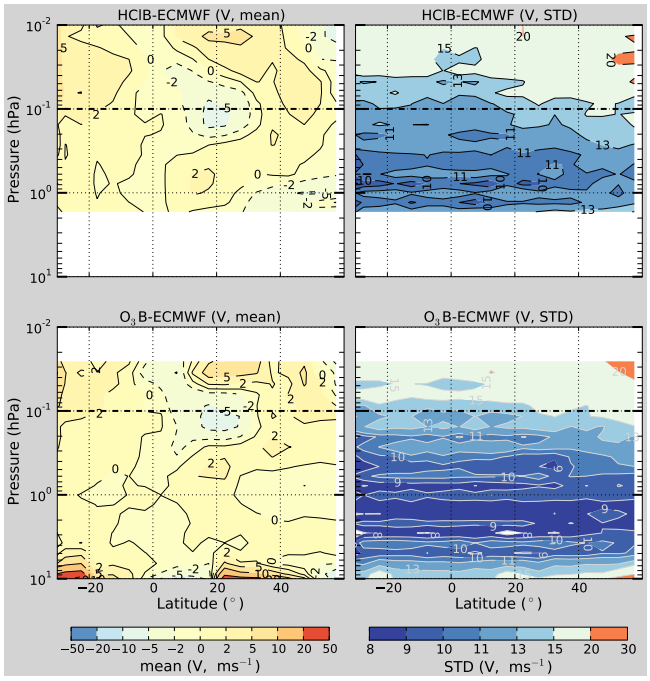

Fig. 8. Comparison of the near meridional winds retrieved from band-B with the operational ECMWF analysis. Data with a line-of-sight orientation between ±10° from the meridional direction are used and ECMWF winds are projected along the line-of-sight direction. Upper panels: mean (left panel) and standard deviation (right panel) of the differences for profiles retrieved from the HCl lines. Lower panels: same as for the upper panels but for profiles retrieved from the O_3 line. Data between November 2009 to April 2010 have been selected.

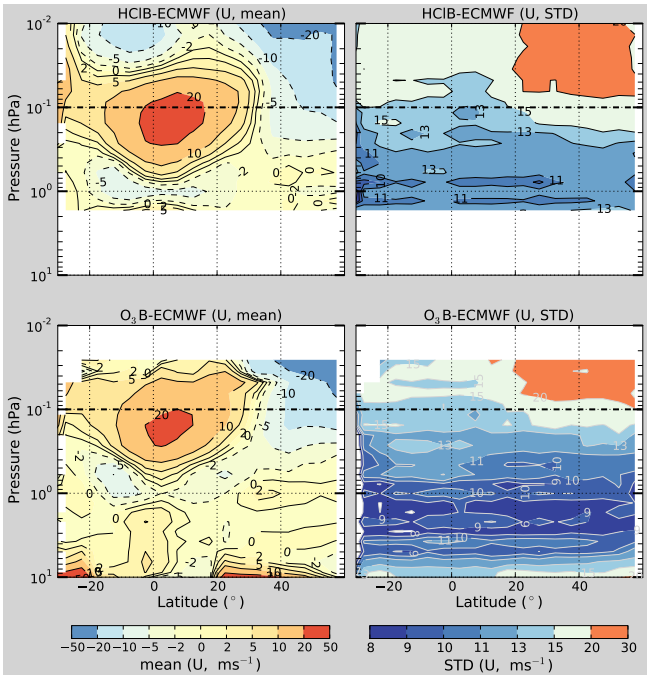

Fig. 9. Same as for Fig. 8 but for the near zonal component. Data with a line-of-sight orientation between ±10° from the zonal direction are used.

For instance Morton et al. (1993) has reported migrating-tides induced meridional wind oscillations above 60 km during the winter solstice and predominantly near 20° N. Below 80 km, the tides amplitude and the vertical wavelength was about 40 $m\,s^{-1}$ and 20 km, respectively.

3.3 Comparison with the ECMWF zonal component

In Fig. 9, the same methodology as in the previous section is applied for deriving the mean and standard deviation of differences between SMILES (band-B) and ECMWF zonal (±10°) winds. Zonal winds are in general significantly larger than the meridional ones, and thus, the results are more sensitive to mismatches due to profile pairing and ECMWF uncertainties.

As for the meridional component, large mean differences, likely due to intensity calibration errors, are found at lower altitudes (> 8 hPa) in the extra-tropical regions (lower right panel) and at latitudes < 30° S because of the fast rotation of the line-of-sight from the zonal to meridional direction. However, in most of the stratosphere (4–1 hPa), a low bias between ±2 $m\,s^{-1}$ is found except over the Equator where the mean difference is between 5–10 $m\,s^{-1}$. In the mesosphere (1–0.01 hPa, upper right panel), a large positive difference (20–30 $m\,s^{-1}$) is found in the tropics and a negative difference at higher northern latitudes (between −20 and −10 $m\,s^{-1}$).

The standard deviations from the middle-stratosphere to lower mesosphere (lower right panel) are slightly higher than the values found for the meridional components. Such an increase of the standard deviation is consistent with the increase of uncertainties in profile-pairing and in ECMWF winds. However, values below 10 $m\,s^{-1}$ are still found over wide regions and more particularly in the extra-tropics indicating that SMILES captured the large variations of the zonal winds (−70 to +70 $m\,s^{-1}$) with a precision which is consistent with the estimation of 7–9 $m\,s^{-1}$. In the tropical mesosphere (0.1–0.01 hPa, upper panels), the standard deviation is between 15 and 20 $m\,s^{-1}$ which also corresponds to the retrieval precision. At northern mid-latitudes, the mesospheric standard deviation significantly increases to 20–30 $m\,s^{-1}$, likely due to the increase of errors in profile-pairing and of the ECMWF analysis itself.

The comparisons of the meridional and zonal winds derived from SMILES with those from ECMWF are a further indication of the quality of the measurements and of the retrieval process. The large differences between the ECMWF and SMILES zonal-winds found in the tropics and in the mesosphere indicate that a future instrument similar to SMILES could significantly improve ECMWF analysis in these regions by assimilating the observations in the model.

Although, the current SMILES observations cover a short period, some persistent biases in the analysis during the whole winter are clearly seen and SMILES could help to understand their origin. In particular, the observations can provide new constraints on the parameterisation of unresolved waves for the analysed winter which might be applied to other years. However, such investigations are out of the scope of this analysis.

4 Examples of the observed wind fields

4.1 Monthly variation of zonal-winds

Figure 10 shows the zonally and monthly averaged zonal-winds obtained from band-B between 30° S–55° N and from mid-October to mid-April. Information at lower altitudes > 0.1 hPa (< 65 km) is retrieved from the O_3 line and that for the upper altitudes is from the HCl triplet. Until the first week of November, ECMWF were not available to us and the zero-wind correction has been calculated with winds from the version 5.2 of the analysis of the Goddard Earth Observing System Data Assimilation System model (GEOS-5.2) (Reinecker, 2008). In November and February, the observed latitude range is displaced to about 60° S–30° N because of the 180°–maneuver of the ISS when hosting the space shuttle. The space shuttle also docked in April, but the viewing geometry did not allow the construction of "zero-wind" profiles. Since the Southern Hemisphere observations corresponded only to a few days, it has been decided to only focus on the region observed in the normal operation mode (30° S–55° N).

The monthly climatology exhibits the main and well known characteristics of the seasonal variations of the zonal-winds. Near the equinoxes (October, March and April), in the stratosphere and the lower mesosphere, zonal-winds are primarily eastward. In December and January, they become stronger with a large inter-hemispheric contrast: eastward in the winter-time Northern Hemisphere and westward in the summer-time Southern Hemisphere.

In the tropical upper-stratosphere and mesosphere (< 3 hPa), the main characteristics of the Semi-Annual-Oscillation (SAO) in the zonal-winds are seen with, in particular, the opposite phase between the stratosphere (westward in December) and the mesosphere (eastward in December). At lower altitudes (> 4 hPa), the SAO signal vanishes and is dominated by the Quasi-Biennal Oscillation (QBO) which is in an easterly phase (westward winds) during that period. The observed tropical SAO is discussed in more details in Sect. 4.3.

Though the Arctic region is not observed by SMILES, the zonal winds in the northernmost mid-latitudes (45–55° N) are high westerlies during winter (e.g. in December and January) revealing the edge of the Arctic polar Vortex. The dynamics of the Arctic winter 2009/2010 have been described

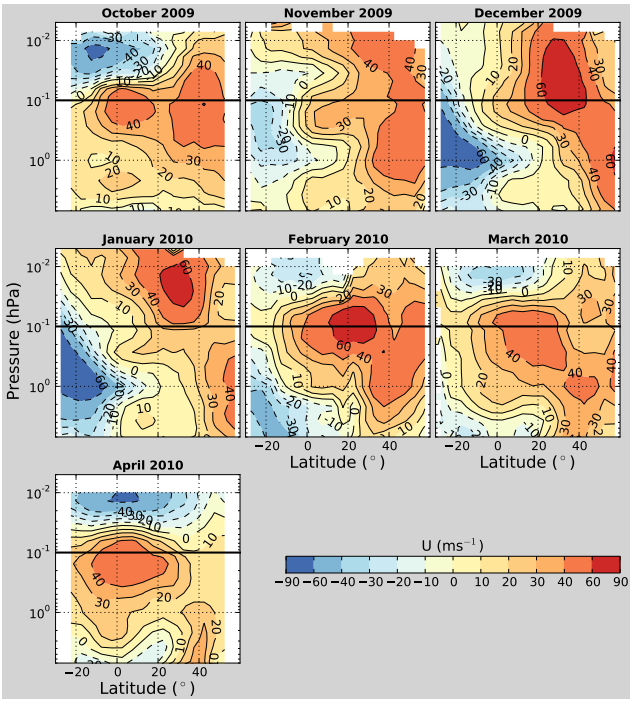

Fig. 10. Monthly and zonally averaged near zonal-wind derived from SMILES measurements in band B between October 2009 to April 2010. Wind information is taken from the O_3 line retrieval for altitudes below 0.1 hPa (65 km) and from the HCl line retrieval above. Data with a line-of-sight orientation between ±10° from the zonal direction are used.

in several studies (Wang and Chen, 2010; Dörnbrack et al., 2012; Kuttippurath and Nikulin, 2012). In early winter, planetary wave activity prevented the formation of a strong vortex in the lower stratosphere and the vortex eventually split at the beginning of December (minor stratospheric warming). From December onward, the vortex became strong throughout the stratosphere until a major sudden stratospheric warming (SSW) occurred on 24–26 January 2010. After this event, a weak vortex reformed and disappeared in April. It is shown in Sect. 4.2 that the effects of the two SSW are observed at 2 hPa in the daily variation of the mean zonal-wind between 50° N and 55° N. Hence, SMILES offers direct wind measurements for studying the SSW development from the mid-stratosphere (8 hPa) to the mesosphere as well as the interactions with the mid-latitudes.

4.2 The sudden stratospheric warming events

The effects of the major SSW at ∼5 hPa (∼36 km) are clearly seen in Fig. 3. The coloured background indicates the abundance of N_2O from a dynamical model driven by ECMWF winds on the 850 K surface and constrained by Odin/SMR observations (Rösevall et al., 2007). The polar vortex is characterised by low values of N_2O (blueish colour) inside and high values (yellow colour) on its border. On

2 January 2010, the vortex is well centred above the polar region and strong eastward winds are measured on its periphery. The meridional component is alternatively southward or northward following the vortex meanders. On 26 January, the vortex is displaced over the north of Europe and it is confined between 60° W and 120° E. Inside the vortex, SMILES observed the change of the direction of the meridional winds due to the counterclockwise rotation of the flow. Outside the vortex a westward flow is measured due to an anti-cyclonic system located above the pacific.

Figure 11 (red dots) shows the daily variation at ∼ 2 hPa of zonally averaged zonal-winds measured between 50–55° N. The time series is made from the O_3 line retrievals. When both bands A and B are measured simultaneously, only band-B is used. The error bars correspond to the daily-mean precision $\bar{e}$ (1-σ):

$$\bar{e} = \sqrt{\frac{e^2}{n_{\text{zero}}} + \frac{e^2 + e_s^2}{n_{\text{wind}}}}, \quad (1)$$

where $e = 5\,\text{m s}^{-1}$ is the single profile retrieval precision at 2 hPa (Sect. 2.2), $e_s = 5\,\text{m s}^{-1}$ is the additional noise arising from the zero-wind correction (Sect. 3.1) and, n_{zero} and n_{wind} are the number of profiles to construct the daily zero-wind and the mean zonal-wind, respectively. The first term below the root-square operator is added to account for the retrieval errors on the zero-wind profiles.

A minor and a major SSW occurred in the beginning of December and at the end of January, respectively. In both cases, a reversal of the mean zonal flow direction is measured between 50–55° N, accompanied by a steep increase of the temperature in the Arctic (blue dashed line). The temperature data are daily and zonally averaged AURA/MLS observations (Schwartz et al., 2008; Limpasuvan et al., 2005) between 60–80° N. The wind and temperature observations are consistent with the analysis of meteorological data in the Arctic of various winters (Labitzke and Kunze, 2009; Manney et al., 2009; Dörnbrack et al., 2012). In the beginning of January, when the vortex had the strongest intensity, the mean eastward zonal-winds strongly increased to 60–80 m s^{-1}. Then, the flow direction gradually changed until the end of January ($-20\,\text{m s}^{-1}$). The flow returned to a normal eastward direction in few days and reached a maximum velocity of 40 m s^{-1} in the beginning of March and decreased again when the vortex disappeared in the springtime.

The ECMWF zonal-winds (Fig. 11, black dots) are consistent with the measurements. A good agreement (difference $< 5\,\text{m s}^{-1}$) is found on average. The largest differences (10–15 m s^{-1}) are found in beginning of November and January when the vortex was strongest.

4.3 Zonal wind development in the tropics

Figure 12 shows the daily-averaged zonal-wind over the Equator (±5°) using the same averaging method as in

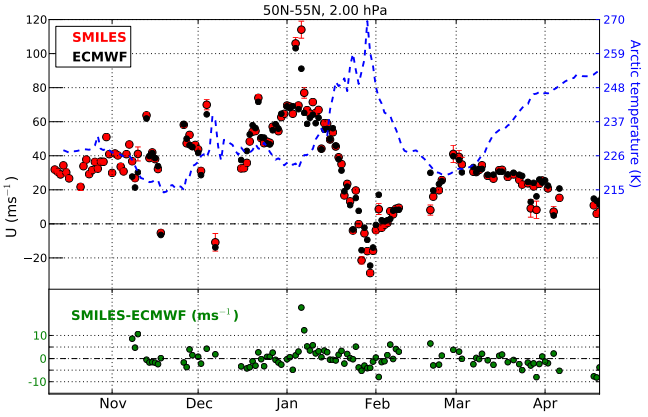

Fig. 11. Upper panel: daily-averaged SMILES zonal-wind in the northern high-latitudes at 2 hPa (∼ 41 km) (red dots) and ECMWF analyses (black dots) between 50–55° N. SMILES winds are retrieved from the O_3 line measured in band-B or in band-A if B is not measured. Data with a line-of-sight orientation between ±10° from the zonal direction are used. ECMWF winds are projected on the line-of-sight. Temperature information (blue dashed line) is based on daily and zonally averaged MLS measurements between 60–80° N. Lower panels: difference SMILES-ECMWF.

Sect. 4.2. When band-B is measured, data above 0.1 hPa are replaced by the HCl line retrievals. The downward progression from the lower mesosphere to the middle stratosphere of the eastward phase (reddish colour) is typical of the winter SAO signal (Hirota, 1980; Garcia et al., 1997). A large variation in amplitude is measured at the stratopause (∼ 1 hPa) where a complete reversal of the wind direction occurred: +20 m s^{-1} (eastward) in November, $-60\,\text{m s}^{-1}$ in January and +20 m s^{-1} in April. In the mesosphere (0.1–0.007 hPa), the dataset, based on the HCl line measured in band-B, is quite sparse. It shows that the wind flow also varies over a large velocity range (between −60 and +60 m s^{-1}) but, as expected, the wind direction changes in anti-phase with the stratosphere (Hitchman et al., 1997; Lossow et al., 2008).

At lower altitudes (below 5 hPa), the SAO amplitude decreases and is mixed with the QBO (Hirota, 1980; Baldwin and Gray, 2005). The westward flow measured over most of the period below 5 hPa is consistent with the easterly (westward) phase of the QBO during the SMILES period. Unfortunately the time period observed is too short to see a full cycle of the QBO.

Figure 13 shows the comparison with ECMWF analysis of daily-averaged zonal-winds at 4, 2 and 0.2 hPa (35, 40, and 60 km) between 15° S–15° N. The error bars correspond to the precision of the daily-averaged profiles (see Sect. 4.2) assuming $e = 7$, 5 and 7 m s^{-1} and $e_s = 7$, 5 and 5 m s^{-1} for the three altitudes, respectively. Southern (left column) and northern tropics (right column) are shown separately in order to account for the asymmetry around the equator: Southern Hemisphere winds are shifted toward the westward direction and the amplitude of the wind variation is larger than that in

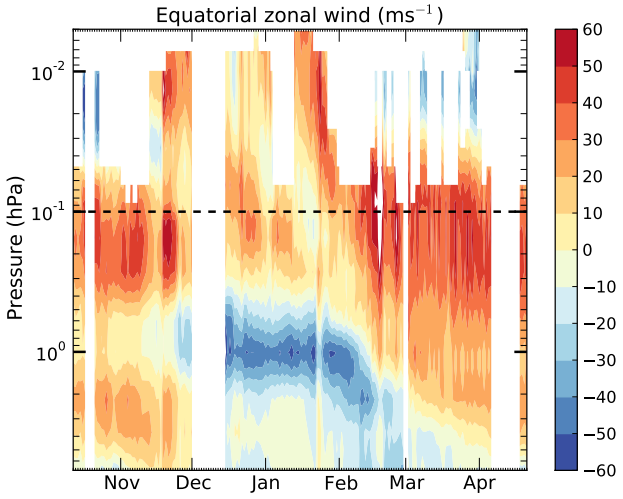

Fig. 12. The Semi-annual oscillation of the zonal winds over the equator (±5°). Red regions correspond to eastward (westerly) winds. The winds from both the ozone and HCl lines are combined in the plot when band-B is measured: information is for O_3 line below 0.1 hPa (65 km) and from HCl above. Information is from O_3 when only band-A is measured. Data with a line-of-sight orientation between ±10° from the zonal direction are used.

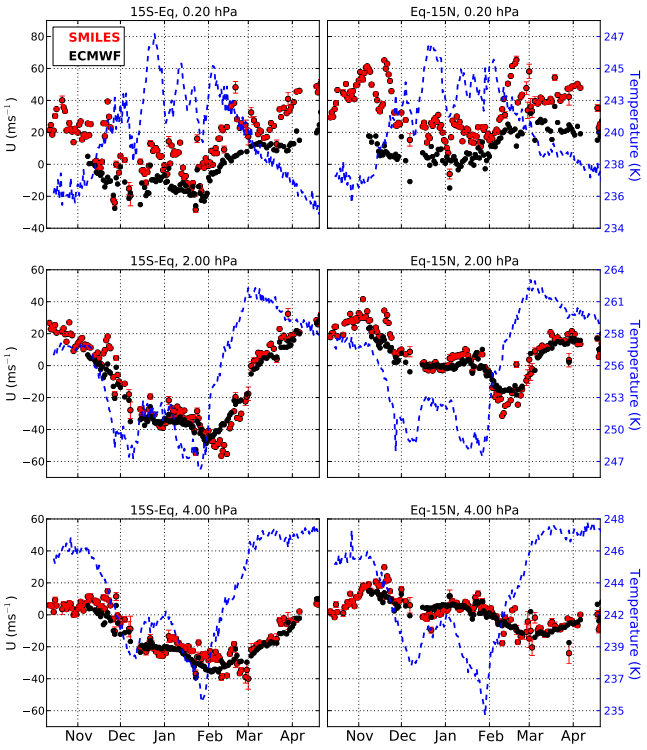

Fig. 13. Left panels: daily-averaged zonal-wind in the southern tropics (15° S–Eq) at 4, 2 and 0.2 hPa (∼35, 41 and 60 km) derived from SMILES measurements (red dots) and ECMWF analyses (black dots). Data are retrieved from the O_3 line in band-B or in band-A if B is not measured. Data with a line-of-sight orientation between ±10° from the zonal direction are used. ECMWF winds are projected on the line-of-sight. The temperature profiles (blue dashed line) is a daily and zonal average of MLS measurements in the same latitudes range. Right panels: same as left panels but for the northern tropics.

the Northern Hemisphere. For instance at 2 hPa, winds vary between −60 and 30 m s^{-1} on the southern side of the equator and between −30 and 40 m s^{-1} on the northern side. Unlike the QBO signal in the zonal wind which is nearly symmetric about the equator (Hamilton et al., 2004), rockets and HRDI observations have reported an asymmetry in the upper-stratospheric SAO with a stronger amplitude in the southern tropics (Hirota, 1980). This is consistent with the SMILES observations. Because of the increase of the SAO with altitude, the wind variation is larger in the upper-stratosphere (2 hPa) than in the mid-stratosphere (4 hPa).

In the stratosphere (4 and 2 hPa), the ECMWF analyses reproduce the measurements fairly well. However, at 2 hPa, the variation range within time intervals as short as about 1 week is larger in the measurements by 20–30 m s^{-1}. In particular, the strong increase of the westward zonal-winds measured during the two first weeks of February in both hemispheres is not seen in the ECMWF analyses. On the contrary, at this time, the ECMWF winds start the westward-to-eastward flow transition. Daily and zonally averaged MLS temperatures for the same latitude range are shown along with the winds. The signature of the SAO in the temperature is in phase with the winds SAO: warmer temperature during the eastward flow and cooler temperature during the westward flow. Note that the transition from the cooler to warmer temperature starts ahead (end of January) compared to the measured westward-to-eastward transition of the zonal winds (beginning of February). It is during this period that the large mismatch between SMILES and ECMWF winds occurs.

In the lower mesosphere (0.2 hPa), the measured wind SAO is in phase with the stratospheric oscillation and the amplitudes in both hemispheres are similar (∼20 m s^{-1}). It is also in phase with the temperature oscillation, which has the opposite phase to that of the stratospheric temperature. The ECMWF winds depart significantly from SMILES winds by a constant offset of about 20 m s^{-1} (consistent with Fig. 9). However, the amplitude of the oscillation is consistent with the observed one. Day-to-day variations are more pronounced in the measurements than in ECMWF winds. In particular, in the Northern Hemisphere, between November and January, the measurements exhibit an oscillation with a period of 10–20 days and an amplitude of ∼20 m s^{-1} which is compatible with a quasi-16 days planetary wave (Lastovicka, 1997). Note that tidal oscillation is aliased with a period of one month (semi-diurnal oscillation) and two months (diurnal oscillation) because of the 2 months precession of the ISS. This must be taken into account for the analysis of the mesospheric wind seasonal variations.

5 Conclusions

We have reported measurements of winds between 8–0.01 hPa and 30° S–55° N during the northern winter 2009–2010. Three winds products were derived from spectroscopic measurements by the sub-mm wave limb sounder JEM/SMILES. The zonal and meridional components were retrieved from different parts of the orbit. The precision and the accuracy are 7–9 $m s^{-1}$ and 2 $m s^{-1}$ between 8–0.5 hPa and $< 20\,m s^{-1}$ and $< 5\,m s^{-1}$ in the mesosphere. The vertical resolution is 5–7 km from the mid-stratosphere to the lower mesosphere and < 20 km elsewhere. To our knowledge, this is the first time that winds have been observed between 35–60 km from space. Internal comparisons show a good quantitative agreement between the different SMILES products. Good agreement is also found with the ECMWF analyses in most of the stratosphere except for the zonal-winds over the equator (mean difference of 5–10 $m s^{-1}$). In the mesosphere SMILES and ECMWF zonal-winds exhibit large differences $> 20\,m s^{-1}$, especially in the tropics. These results demonstrate that SMILES measurements have the potential to significantly improve the capability of atmospheric models to predict winds in the tropical mid- and upper stratosphere, and in the mesosphere in general.

In coming work, SMILES mesospheric winds will be validated using ground-based radar observations. We also expect better retrievals thanks to improvements of the calibrated radiances and spectrometer frequencies spectra (Ochiai et al., 2012c; Mizobuchi et al., 2012a), and of the inversion methodology (e.g. joint inversion of different lines and bands). The aim is to reliably retrieve winds down to 20–25 km which is the theoretical limit for the SMILES measurements. In the mesosphere, the number of retrieved profiles can be increased by the use of the $H^{37}Cl$ lines measured in band-A (though weaker than the band-B $H^{35}Cl$ line) and by using the nighttime O_3 line signal enhancement due to the large chemical diurnal variation of O_3 at altitudes between 0.01–0.005 hPa.

Although the SMILES instrument was not designed for wind measurement, the retrieval performances are close to those used in Lahoz et al. (2005) for stressing the importance of stratospheric wind measurements (error $< 5\,m s^{-1}$ between 25–40 km). This indicates that a carefully designed sub-mm wave radiometer, which is mature technology, has the potential to significantly improve the prediction of wind in atmospheric models and to fill the altitude gap in the stratospheric wind measurements. The optimal specifications and the performances for such instrument are under study.

Appendix A

Retrieval procedure

The wind retrieval uses the algorithms version 2.1.5 developed for retrieving temperature and gas profiles in the SMILES level-2 research chain developed in NICT (http://smiles.nict.go.jp/pub/data/products.html). They are based on the standard least-squares method constrained by an a priori knowledge of the retrieved parameters. A zero profile is used for the wind a priori. The line-of-sight wind information is derived in a two step process using the ozone and HCl lines available in the spectra. Firstly the profiles of atmospheric constituent relevant for the spectral region, temperature and spectrum tangent-height are retrieved disregarding any spectral shifts due to the wind which has no significant impact on the results. Then the wind is retrieved on a 5 km vertical grid by initialising the inversion using the parameters retrieved in the first step. The vertical sampling of the retrieval grid is consistent with the information content of the spectra. Note that at the initialisation step, baseline parameters, i.e. additional radiance offset and slope used to improve the measurement fit, are set to 0. Since, a small baseline is usually retrieved for good SMILES scans, the initial χ^2 (Baron et al. (2011), Eq. 2) has a relatively small value between 20–40.

The two inversion processes use a spectral window of 500 MHz around the chosen molecular lines. The forward model has been modified to include the Doppler frequency shift induced by the air parcels velocity and to compute the wind weighting functions. The frequency shift induced by the wind is included as a change of the spectroscopic lines frequency. The wind weighting functions are computed with a perturbation method for the derivation of the absorption coefficient and with an analytic derivation of a discrete form of the radiative transfer equation (Urban et al., 2004). The frequency dependence of the source function (the Planck function) is neglected and we assume horizontal winds along the full line-of-sight which is only true at the tangent point. Both approximations have a negligible impact on the retrieved velocities in the altitude range considered in the analysis.

Acknowledgements. The SMILES project is jointly led by the Japan Aerospace Exploration Agency (JAXA) and the National Institute of Information and Communications Technology (NICT, Japan). SMILES Data processing was performed with the NICT Science Cloud as a collaborative research project. We acknowledge the European Centre for Medium Range Weather Forecasts (ECMWF) and the Global Modelling and Assimilation Office (GMAO) at NASA Goddard Space Flight Center for access to model results. D. P. Murtagh and J. Urban would like to thank the Swedish National Space Board for support. P. Baron would like to thank K. Muranaga, T. Haru and S. Usui from Systems Engineering Consultants Co. (SEC) for their important contributions to the SMILES project. P. Baron would like to thank Yvan Orsolini for fruitful discussions as well as the two unknown referees and the editor for their comments and suggestions for improving the manuscript.

Edited by: A. Geer

References

Alcaydé, D. and Fontanari, J.: Neutral temperature and winds from EISCAT CP-3 observations, J. Atmos. Terr. Phys., 48, 931–947, 1986.

Alexander, M. J., Geller, M., McLandress, C., Polavarapu, S., Preusse, P., Sassi, F., Sato, K., Eckermann, S., Ern, M., Hertzog, A., Kawatani, Y., Pulido, M., Shaw, T. A., Sigmond, M., Vincent, R., and Watanabe, S.: Recent developments in gravity-wave effects in climate models and the global distribution of gravity-wave momentum flux from observations and models, Q. J. Roy. Meteor. Soc., 136, 1103–1124, doi:10.1002/qj.637, 2010.

Baldwin, M. P. and Dunkerton, T. J.: Propagation of the Arctic oscillation from the stratosphere to the troposphere, J. Geophys. Res., 104, 30937–30946, doi:10.1029/1999JD900445, 1999.

Baldwin, M. P. and Gray, L. J.: Tropical stratospheric zonal winds in ECMWF ERA-40 reanalysis, rocketsonde data, and rawinsonde data, Geophys. Res. Lett., 32, L09806, doi:10.1029/2004GL022328, 2005.

Baldwin, M., Thompson, D., Shuckburgh, E., Norton, W., and Gillett, N.: Weather from the stratosphere?, Science, 301, 317–318, 2003.

Baron, P., Urban, J., Sagawa, H., Möller, J., Murtagh, D. P., Mendrok, J., Dupuy, E., Sato, T. O., Ochiai, S., Suzuki, K., Manabe, T., Nishibori, T., Kikuchi, K., Sato, R., Takayanagi, M., Murayama, Y., Shiotani, M., and Kasai, Y.: The Level 2 research product algorithms for the Superconducting Submillimeter-Wave Limb-Emission Sounder (SMILES), Atmos. Meas. Tech., 4, 2105–2124, doi:10.5194/amt-4-2105-2011, 2011.

Derber, J. and Bouttier, F.: A reformulation of the background error covariance in the ECMWF global data assimilation system, Tellus A, 51, 195–221, doi:10.1034/j.1600-0870.1999.t01-2-00003.x, 1999.

Dörnbrack, A., Pitts, M. C., Poole, L. R., Orsolini, Y. J., Nishii, K., and Nakamura, H.: The 2009–2010 Arctic stratospheric winter – general evolution, mountain waves and predictability of an operational weather forecast model, Atmos. Chem. Phys., 12, 3659–3675, doi:10.5194/acp-12-3659-2012, 2012.

Fleming, E. L., Chandra, S., Barnett, J., and Corney, M.: Zonal mean temperature, pressure, zonal wind and geopotential height as functions of latitude, Adv. Space Res., 10, 11–59, 1990.

Garcia, R. R., Dunkerton, T. J., Lieberman, R. S., and Vincent, R. A.: Climatology of the semiannual oscillation of the tropical middle atmosphere, J. Geophys. Res., 102, 26019–26032, 1997.

Hamilton, K.: Dynamics of the tropical middle atmosphere: a tutorial review, Atmos. Ocean, 36, 319–354, 1998.

Hamilton, K., Hertzog, A., Vial, F., and Stenchikov, G.: Longitudinal Variation of the Stratospheric Quasi-Biennial Oscillation, J. Atmos. Sci., 61, 383–402, 2004.

Hays, P. B., Abreu, V. J., Dobbs, M. E., Gell, D. A., Grassl, H. J., and Skinner, W. R.: The High-Resolution Doppler Imager on the upper-atmosphere research satellite, J. Geophys. Res., 98, 10713–10723, 1993.

Hildebrand, J., Baumgarten, G., Fiedler, J., Hoppe, U.-P., Kaifler, B., Lübken, F.-J., and Williams, B. P.: Combined wind measurements by two different lidar instruments in the Arctic middle atmosphere, Atmos. Meas. Tech., 5, 2433–2445, doi:10.5194/amt-5-2433-2012, 2012.

Hirota, I.: Observational evidence of the semiannual oscillation in the tropical middle atmosphere: a review, Pure Appl. Geophys., 118, 217–238, 1980.

Hitchman, M. H., Kudeki, E., Fritts, D. C., Kugi, J. M., Fawcett, C., Postel, G. A., Yao, C. Y., Ortland, D., Riggin, D., and Harvey, V. L.: Mean winds in the tropical stratosphere and mesosphere during January 1993, March 1994, and August 1994, J. Geophys. Res., 102, 26033–26052, 1997.

Holton, J. R. and Alexander, M. J.: The role of waves in the transport circulation of the middle atmosphere, in: Geophys. Monogr. Ser., vol. 123, AGU, Washington DC, 21–35, 2000.

Isaksen, L., Bonavita, M., Buizza, R., Fisher, M., Haseler, J., Leutbecher, M. and Raynaud, L.: Ensemble of data assimilations at ECMWF, ECMWF Technical Memorandum 636, available at: http://www.ecmwf.int/publications/library/do/references/show?id=90034, 2010.

Jacobi, C., Arras, C., Kürschner, D., Singer, W., Hoffmann, P., and Keuer, D.: Comparison of mesopause region meteor radar winds, medium frequency radar winds and low frequency drifts over Germany, Adv. Space Res., 43, 247–252, 2009.

Kasai, Y. J., Urban, J., Takahashi, C., Hoshino, S., Takahashi, K., Inatani, J., Shiotani, M., and Masuko, H.: Stratospheric ozone isotope enrichment studied by submillimeter wave heterodyne radiometry: observation capabilities of SMILES, IEEE T. Geosci. Remote, 44, 676–693, 2006.

Kasai, Y., Sagawa, H., Kreyling, D., Suzuki, K., Dupuy, E., Sato, T. O., Mendrok, J., Baron, P., Nishibori, T., Mizobuchi, S., Kikuchi, K., Manabe, T., Ozeki, H., Sugita, T., Fujiwara, M., Irimajiri, Y., Walker, K. A., Bernath, P. F., Boone, C., Stiller, G., von Clarmann, T., Orphal, J., Urban, J., Murtagh, D., Llewellyn, E. J., Degenstein, D., Bourassa, A. E., Lloyd, N. D., Froidevaux, L., Birk, M., Wagner, G., Schreier, F., Xu, J., Vogt, P., Trautmann, T., and Yasui, M.: Validation of stratospheric and mesospheric ozone observed by SMILES from International Space Station, Atmos. Meas. Tech. Discuss., 6, 2643–2720, doi:10.5194/amtd-6-2643-2013, 2013.

Khosravi, M., Baron, P., Urban, J., Froidevaux, L., Jonsson, A. I., Kasai, Y., Kuribayashi, K., Mitsuda, C., Murtagh, D. P., Sagawa, H., Santee, M. L., Sato, T. O., Shiotani, M., Suzuki, M., von Clarmann, T., Walker, K. A., and Wang, S.: Diurnal variation of stratospheric HOCl, ClO and HO_2 at the equator: comparison of 1-D model calculations with measurements of satellite instruments, Atmos. Chem. Phys. Discuss., 12, 21065–21104, doi:10.5194/acpd-12-21065-2012, 2012.

Kikuchi, K., Nishibori, T., Ochiai, S., Ozeki, H., Irimajiri, Y., Kasai, Y., Koike, M., Manabe, T., Mizukoshi, K., Murayama, Y., Nagahama, T., Sano, T., Sato, R., Seta, M., Takahashi, C., Takayanagi, M., Masuko, H., Inatani, J., Suzuki, M., and Shiotani, M.: Overview and early results of the Superconducting Submillimeter-Wave Limb-Emission Sounder (SMILES), J. Geophys. Res., 115, D23306, doi:10.1029/2010JD014379, 2010.

Killeen, T. L., Skinner, W. R., Johnson, R. M., Edmonson, C. J., Wu, Q., Niciejewski, R. J., Grassl, H. J., Gell, D. A., Hansen, P. E., Harvey, J. D., and Kafkalidis, J. F.: TIMED Doppler Interferometer (TIDI), optical spectroscopic techniques and instrumentation for atmospheric and space research III, Proc. SPIE, 3756, 289–301, doi:10.1117/12.366383, 1999.

Kuttippurath, J. and Nikulin, G.: A comparative study of the major sudden stratospheric warmings in the Arctic winters

2003/2004–2009/2010, Atmos. Chem. Phys., 12, 8115–8129, doi:10.5194/acp-12-8115-2012, 2012.

Labitzke, K. and Kunze, M.: On the remarkable Arctic winter in 2008/2009, J. Geophys. Res., 114, D00I02, doi:10.1029/2009JD012273, 2009.

Lahoz, W. A., Brugge, R., Jackson, D. R., Migliorini, S., Swinbank, R., Lary, D., and Lee, A.: An observing system simulation experiment to evaluate the scientific merit of wind and ozone measurements from the future SWIFT instrument, Q. J. Roy. Meteor. Soc., 131, 503–523, 2005.

Lastovicka, J.: Observations of tides and planetary waves in the atmosphere-ionosphere system, Adv. Space Res., 20, 1209–1222, doi:10.1016/S0273-1177(97)00774-6, 1997.

Limpasuvan, V., Wu, D. L., Schwartz, M. J., Waters, J. W., Wu, Q., and Killeen, T. L.: The two-day wave in EOS MLS temperature and wind measurements during 2004–2005 winter, Geophys. Res. Lett., 32, L17809, doi:10.1029/2005GL023396, 2005.

Lossow, S., Urban, J., Gumbel, J., Eriksson, P., and Murtagh, D.: Observations of the mesospheric semi-annual oscillation (MSAO) in water vapour by Odin/SMR, Atmos. Chem. Phys., 8, 6527–6540, doi:10.5194/acp-8-6527-2008, 2008.

Maekawa, Y., Fukao, S., Yamamoto, M., Yamanaka, M. D., Tsuda, T., Kato, S., and Woodman, R. F.: First observation of the upper stratospheric vertical wind velocities using the Jicamarca VHF radar, Geophys. Res. Lett., 20, * 2235–2238, doi:10.1029/93GL02606, 1993.-

Manney, G. L., Schwartz, M. J., Krüger, K., Santee, M. L., Pawson, S., Lee, J. N., Daffer, W. H., Fuller, R. A., and Livesey, N. J.: Aura Microwave Limb Sounder observations of dynamics and transport during the record-breaking 2009 Arctic stratospheric major warming, Geophys. Res. Lett., 36, L12815, doi:10.1029/2009GL038586, 2009.

Marshall, A. G. and Scaife, A. A.: Impact of the QBO on surface winter climate, J. Geophys. Res., 114, D18110, doi:10.1029/2009JD011737, 2009.

McDade, I. C., Shepherd, G. G., Gault, W. A., Rochon, Y. J., McLandress, C., Scott, A., Rowlands, N., and Buttner, G.: The stratospheric wind interferometer for transport studies SWIFT), in: Igarss 2001: Scanning the Present and Resolving the Future, Vol. 3, Proceedings, 1344–1346, Sydney NSW, 9–13 July, doi:10.1109/IGARSS.2001.976839, 2001.

Merino, F., Murtagh, D., Ridal, M., Eriksson, P., Baron, P., Ricaud, P., and de la Noe, J.: Studies for the Odin Sub-Millimetre Radiomoter: III. Performance simulations, Can. J. Phys., 80, 357–373, doi:10.1139/P01-154, 2002.

Mizobuchi, S., Ozeki, H., Kikuchi, K., Ochiai, S., Baron, P., and Nishibori, T.: Improvement in calibration algorithm of the AOS (acousto-optical spectrometer) using in-orbit measurement data, Geoscience and Remote Sensing Symposium (IGARSS), 2012 IEEE Internationa 4695–4698, doi:10.1109/IGARSS.2012.6350417, available at: http://igarss12.org/, 2012a.

Mizobuchi, S., Kikuchi, K., Ochiai, S., Nishibori, T., Sano, T., Tamaki, K., and Ozeki, H.: In-orbit measurement of the AOS (Acousto-Optical Spectrometer) response using frequency comb signals, IEEE J. Sel. Top. Appl., 5, 977–983, doi:10.1109/JSTARS.2012.2196413, 2012b.

Morton, Y. T., Lieberman, R. S., Hays, P. B., Ortland, D. A., Marshall, A. R., Wu, D., Skinner, W. R., Burrage, M. D., Gell, D. A., and Yee, J.-H.: Global mesospheric tidal winds observed by the high resolution Doppler imager on board the Upper Atmosphere Research Satellite, Geophys. Res. Lett., 20, 1263–1266, doi:10.1029/93GL00826, 1993.

Nezlin, Y., Rochon, Y., and Polavarapu, S.: Impact of tropospheric and stratospheric data assimilation on mesospheric prediction, Tellus A, 61, 154–159, doi:10.1111/j.1600-0870.2008.00368.x, 2009.

Niciejewski, R., Wu, Q., Skinner, W., Gell, D., Cooper, M., Marshall, A., Killeen, T., Solomon, S., and Ortland, D.: TIMED Doppler interferometer on the Thermosphere Ionosphere Mesosphere Energetics and Dynamics satellite: data product overview, J. Geophys. Res.-Space, 111, A11S90, doi:10.1029/2005JA011513, 2006.

Ochiai, S., Kikuchi, K., Nishibori, T., and Manabe, T.: Gain nonlinearity calibration of submillimeter radiometer for JEM/SMILES, IEEE J. Sel. Top. Appl., 5, 962–969, doi:10.1109/JSTARS.2012.2193559, 2012a.

Ochiai, S., Kikuchi, K., Nishibori, T., Manabe, T., Ozeki, Hiroyuki Mizobuchi, S., and Irimajiri, Y.: Receiver performance of Superconducting Submillimeter-Wave Limb-Emission Sounder (SMILES) on the international space station, IEEE T. Geosci. Remote, 99, 1–12, doi:10.1109/TGRS.2012.2227758, 2012b.

Ochiai, S., Nishibori, T., Kikuchi, K., Mizobuchi, S., Manabe, T., Mitsuda, C., Baron, P., and Ueno, S.: Tangent height accuracy of superconducting Submillimeter-Wave Limb-Emission Sounder (SMILES) on International Space Station (ISS), Geoscience and Remote Sensing Symposium (IGARSS), 2012 IEEE International, 1290–1293, doi:10.1109/IGARSS.2012.6350824, available at: http://igarss12.org/, 2012c.

Orr, A., Bechtold, P., Scinocca, J., Ern, M., and Janiskova, M.: Improved Middle Atmosphere Climate and Forecasts in the ECMWF Model through a Nonorographic Gravity Wave Drag Parameterization, J. Climate, 23, 5905–5926, 2010.

Ortland, D. A., Skinner, W. R., Hays, P. B., Burrage, M. D., Lieberman, R. S., Marshall, A. R., and Gell, D. A.: Measurements of stratospheric winds by the High Resolution Doppler Imager, J. Geophys. Res., 101, 10351–10363, 1996.

Polavarapu, S., Shepherd, T. G., Rochon, Y., and Ren, S.: Some challenges of middle atmosphere data assimilation, Q. J. Roy. Meteor. Soc., 131, 3513–3527, doi:10.1256/qj.05.87, 2005.

Randel, W., Udelhofen, P., Fleming, E., Geller, M., Gelman, M., Hamilton, K., Karoly, D., Ortland, D., Pawson, S., Swinbank, R., Wu, F., Baldwin, M., Chanin, M.-L., Keckhut, P., Labitzke, K., Remsberg, E., Simmons, A., and Wu, D.: The SPARC Intercomparison of Middle-Atmosphere Climatologies, J. Climate, 17, 986–1003, doi:10.1175/1520-0442(2004)017<0986:TSIOMC>2.0.CO;2, 2004.

Reinecker, M.: The GEOS-5 data assimilation system: A documentation of GEOS-5.0, Tech Report 104606 V27, NASA, 2008.

Rösevall, J. D., Murtagh, D. P., Urban, J., and Jones, A. K.: A study of polar ozone depletion based on sequential assimilation of satellite data from the ENVISAT/MIPAS and Odin/SMR instruments, Atmos. Chem. Phys., 7, 899–911, doi:10.5194/acp-7-899-2007, 2007.

Rüfenacht, R., Kämpfer, N., and Murk, A.: First middle-atmospheric zonal wind profile measurements with a new ground-based microwave Doppler-spectro-radiometer, Atmos. Meas. Tech., 5, 2647–2659, doi:10.5194/amt-5-2647-2012,

2012.

Schwartz, M. J., Lambert, A., Manney, G. L., Read, W. G., Livesey, N. J., Froidevaux, L., Ao, C. O., Bernath, P. F., Boone, C. D., Cofield, R. E., Daffer, W. H., Drouin, B. J., Fetzer, E. J., Fuller, R. A., Jarnot, R. F., Jiang, J. H., Jiang, Y. B., Knosp, B. W., Krüger, K., Li, J.-L. F., Mlynczak, M. G., Pawson, S., Russell, J. M., I., Santee, M. L., Snyder, W. V., Stek, P. C., Thurstans, R. P., Tompkins, A. M., Wagner, P. A., Walker, K. A., Waters, J. W., and Wu, D. L.: Validation of the Aura Microwave Limb Sounder temperature and geopotential height measurements, J. Geophys. Res., 113, D15S11, doi:10.1029/2007JD008783, 2008.

Shepherd, G. G., Thuillier, G., Gault, W. A., Solheim, B. H., Hersom, C., Alunni, J. M., Brun, J. F., Brune, S., Charlot, P., Cogger, L. L., Desaulniers, D. L., Evans, W. F. J., Gattinger, R. L., Girod, F., Harvie, D., Hum, R. H., Kendall, D. J. W., Llewellyn, E. J., Lowe, R. P., Ohrt, J., Pasternak, F., Peillet, O., Powell, I., Rochon, Y., Ward, W. E., Wiens, R. H., and Wimperis, J.: WINDII, The wind imaging interferometer on the upper-atmosphere research satellite, J. Geophys. Res., 98, 10725–10750, 1993.

Shepherd, T. G.: Transport in the middle atmosphere, J. Meteorol. Soc. Jpn. II, 85B, 165–191, 2007.

Shepherd, T. G.: Dynamics, stratospheric ozone, and climate change, Atmos. Ocean, 46, 117–138, doi:10.3137/ao.460106, 2008.

Sigmond, M., Scinocca, J. F., and Kushner, P. J.: Impact of the stratosphere on tropospheric climate change, Geophys. Res. Lett., 35, L12706, doi:10.1029/2008GL033573, 2008.

Stoffelen, A., Pailleux, J., Källén, E., Vaughan, J., Isaksen, L., Flamant, P., Wergen, W., Andersson, E., Schyberg, H., Culoma, A., Meynart, R., Endemann, M., and Ingmann, P.: The atmospheric dynamics mission for global wind field measurement, B. Am. Meteorol. Soc., 86, 73–87, 2005.

Swinbank, R. and Ortland, D. A.: Compilation of wind data for the Upper Atmosphere Research Satellite (UARS) Reference Atmosphere Project, J. Geophys. Res., 108, 4615, 2003.

Takahashi, C., Ochiai, S., and Suzuki, M.: Operational retrieval algorithms for JEM/SMILES level 2 data processing system, J. Quant. Spectrosc. Ra., 111, 160–173, doi:10.1016/j.jqsrt.2009.06.005, 2010.

Urban, J., Baron, P., Lautie, N., Schneider, N., Dassas, K., Ricaud, P., and De La Noe, J.: MOLIERE (v5): a versatile forward- and inversion model for the millimeter and submillimeter wavelength range, J. Quant. Spectrosc. Ra., 83, 529–554, doi:10.1016/S0022-4073(03)00104-3, 2004.

Wang, L. and Chen, W.: Downward Arctic Oscillation signal associated with moderate weak stratospheric polar vortex and the cold December 2009, Geophys. Res. Lett., 37, L09707, doi:10.1029/2010GL042659, 2010.

Wu, D. L., Schwartz, M. J., Waters, J. W., Limpasuvan, V., Wu, Q. A., and Killeen, T. L.: Mesospheric doppler wind measurements from Aura Microwave Limb Sounder (MLS), Adv. Space Res., 42, 1246–1252, 2008.

Žagar, N., Gustafsson, N., and Källén, E.: Variational data assimilation in the tropics: the impact of a background-error constraint, Q. J. Roy. Meteor. Soc., 130, 103–125, doi:10.1256/qj.03.13, 2004.